Statistics of bubble rearrangements in a slowly sheared two-dimensional foam

Michael Dennin
Department of Physics and Astronomy, University of California at Irvine, Irvine, California 92697-4575
(Received 26 May 2004; published 28 October 2004)

Many physical systems exhibit plastic flow when subjected to slow steady shear. A unified picture of plastic flow is still lacking; however, there is an emerging theoretical understanding of such flows based on irreversible motions of the constituent "particles" of the material. Depending on the specific system, various irreversible events have been studied, such as T1 events in foam and shear transformation zones (STZ's) in amorphous solids. This paper presents an experimental study of the T1 events in a model, two-dimensional foam: bubble rafts. In particular, I report on the connection between the distribution of T1 events and the behavior of the average stress and average velocity profiles during both the initial elastic response of the bubble raft and the subsequent plastic flow at sufficiently high strains.

DOI: 10.1103/PhysRevE.70.041406 PACS number(s): 82.70.−y, 83.60.La, 62.20.Fe

I. INTRODUCTION

Bubble rafts have been used as a model experimental system for the study of crystalline and amorphous solids [1–3] and for the study of two-dimensional foam [4,5]. This overlap is just one of many examples that points to an important question in the study of the mechanical response of materials. Under conditions of slow steady shear, what, if any, is the connection between the response of "mesoscopic" materials, such as foams, emulsions, pastes, and slurries, and plastic flow of "molecular" systems, such as amorphous solids? Based on macroscopic measurements, the systems are similar. There is an initial elastic response for small strains (or stresses) and a yield stress, above which irreversible deformations, or plastic deformations, occur. Eventually, above some critical stress (or strain), the system enters a "flowing" state that is characterized by irregular periods of stress increase and decrease. This is often referred to as unbounded plastic flow. For the purposes of this paper, this will simply be referred to as plastic flow. As one reduces the shear rate, the critical stress approaches the yield stress in such a way that for sufficiently slow shear rates, the behavior of the system is essentially shear-rate-independent. This is often referred to as the *quasistatic regime*. A complete "microscopic" picture of plastic flow still does not exist, where microscopic refers to the fundamental length scale relevant to the system in question. For example, in bubble rafts, it would be the dynamics of individual bubbles. Open questions include the microscopic source of the stress release events, the spatial and temporal distribution of such events, and the nature of such events during periods of stress increase. Experimentally, the challenge is identifying systems for which the microscopic events are directly observable. This is one of the main advantages of mesoscopic systems, such as the bubble raft, and the reason for the interest in making connections between mesoscopic systems and molecular systems, such as amorphous solids.

Models and simulations of diverse systems, ranging from solids [6–13] to foam [14–23], have provided a number of insights into these questions. The focus of this paper is on the role of T1 events in foam. Aqueous foam consists of gas bubbles separated by liquid walls [24–26]. A T1 event is an irreversible neighbor switching event. Both a schematic representation and an actual T1 event are presented in Fig. 1. For the purposes of this paper, I will focus on the role of T1 events during the steady shear of foam. However, it should be mentioned that understanding the nonlinear events that are *not* shear induced may be important when comparing foam and amorphous solids. In the absence of external stress, foam coarsens, and T1 events occur due to geometric changes in the foam structure. These T1 events are not necessarily distinguishable from those caused by flow. In con-

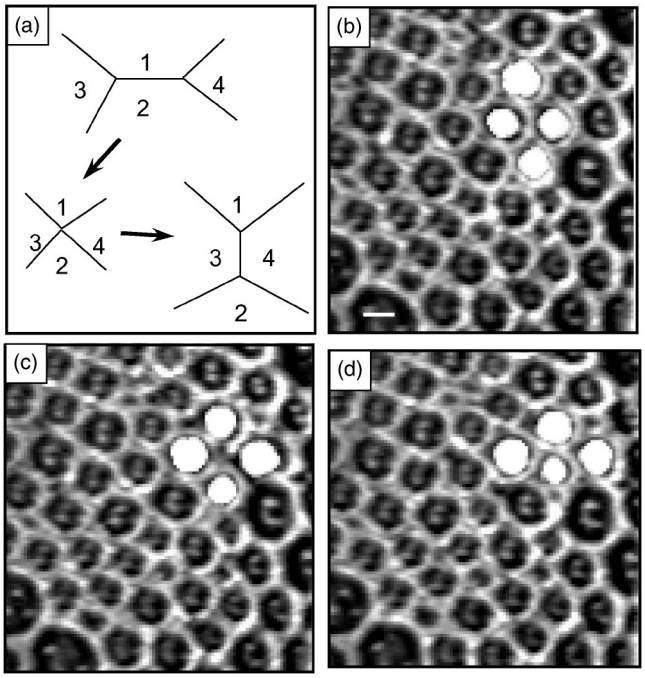

FIG. 1. (a) Schematic representation of the three main steps in a T1 event. The bubbles labeled 1 and 2 are initially neighbors. As the bubbles are sheared, all four bubbles meet at a vertex. After the event, the bubbles labeled 3 and 4 are neighbors. (b)–(d) are three images illustrating an actual T1 event in the bubble raft. The location of one T1 event is highlighted by artificially coloring the bubbles involved white. The images are taken 3.2 s apart and the white scale bar in (b) is 2 mm long.

trast, most amorphous solids do not exhibit the equivalent of coarsening. However, thermally activated events may be important. Possible differences between thermally activated and coarsening events raise interesting questions, but they are beyond the scope of this paper.

Simulations of flowing foam have characterized different aspects of T1 events. Often, one separately considers T1 events and "avalanches," i.e., sudden releases of stress (or energy) in the foam. One issue is whether or not the probability of the number of T1 events in a given avalanche exhibits power-law behavior. A common model to study dry foam (where the bubbles are essentially polygonal) is the vertex model [14–16]. In the vertex model, a T1 event is defined to occur when the distance between two vertices (i.e., the wall between two bubbles) is below a threshold value. One then eliminates this wall, creating a T1 event. Therefore, within this model, all T1 events are essentially instantaneous. In this case, simulations found evidence for power-law behavior of the probability of T1 events. Another characterization of the T1 events is the number of T1 events per bubble per unit strain, R_{T1}. For the vertex model, this quantity is $R_{T1}=0.5$. A modified version of the vertex model has been used to study the issue of flow localization under shear [23]. These simulations report a correlation between the spatial localization of T1 events to the neighborhood of a system boundary with the localization of shear in the same region. The issue of shear localization will be discussed in more detail later.

Another class of models focuses on wet foam (foam in which the bubbles are essentially spherical, or, in two dimensions, circular), using a quasistatic simulation [19,20]. These simulations involve making a small step strain and then allowing the system to relax to an energy minimum before applying the next step strain. Anytime the energy decreases after a step strain, one declares this an "avalanche" or "event." By comparing neighbors in the initial and final state, one can count the number of T1 events for a particular avalanche. In these simulations, avalanches consisting of a large number of T1 events were observed, suggesting the possibility of power-law behavior [19,20]. For this model, R_{T1} was not reported.

Wet foam under steady shear has also been simulated using a q-Potts model [21]. In this case, different bubbles are identified by different spin orientations. Simulations of the q-Potts model find that the distribution of topological rearrangements is not power-law-like. However, the distribution of energy drops may be consistent with power-law behavior [21].

Another important set of simulations for wet foam involved studying the steady shear of the bubble model [17,18,22]. This model treats bubbles as spheres (or circles) that interact via a spring force proportional to their overlap and a viscous drag proportional to velocity differences. As this model directly simulates dynamics, the duration of T1 events exhibits a distribution of duration times. Simulations focused on small shear rates in the quasistatic limit, i.e., the flow properties were independent of the shear rate. Under these conditions, no evidence of power-law behavior is observed in the bubble model at high bubble density, and $R_{T1}=0.15$ [17,18,22]. If one decreases the density of the bubbles, it appears that the distribution of events approaches a power law as one approaches the critical density for the "melting" of the foam [22].

Before discussing the current state of experiments in foam, it is useful to put the theoretical work on T1 events in foam in the context of two points of view of plasticity in amorphous materials. First, the idea of shear transformation zones (STZ's), as developed by Falk and Langer [6], has received significant attention. STZ are a way of describing local, irreversible rearrangements of particles during shear. STZ are based on previous work by Spaepen and Argon on activated transitions and Turnball, Cohen, and others on free-volume fluctuations. As the STZ refers to a small region of the material with certain properties [27], there is only a loose connection between the STZ and T1 events. However, it is reasonable to identify as an STZ regions in which a few T1 events combine to form a local slip [see, for instance, Fig. 5(e)]. It is expected that the local rearrangements identified as STZ are associated with quadrupolar energy fluctuations. In fact, the expected quadrupolar energy fluctuations have been observed associated with T1 events in a simulation of foam [23], but not, as of yet, in simulations of molecular systems.

Another view of plasticity is based on shear induced changes in the potential energy landscape, as proposed by Malandro and Lacks [28]. This picture derives from an inherent structure formalism and focuses on changes in the macroscopic mechanical response of a material due to shear induced changes of the potential energy. This formalism has been used to study simulations of a quasistatic version of the bubble model [29]. In this case, systemwide rearrangement events are observed. This is not seen in bubble model simulations of the quasistatic limit, but it is seen in other quasistatic simulations of foam. The work in Ref. [29] suggests the need to carefully define the concept of an "event," especially for steady-state experiments where the time scale for events to occur relative to the applied shear can be important. For example, a shear-rate regime may exist that is quasistatic as defined by the behavior of quantities such as the average stress, but not quasistatic with regard to the duration of stress releases. Hence, large events get "broken up" by the steady shear, changing the nature of the distribution of events.

A number of experimental studies of bubble rearrangements in model foam have been carried out. As mentioned, some of the earliest work was done using bubble rafts [1–3], i.e., layers of gas bubbles floating on a liquid surface, as a model molecular system, both for crystalline and amorphous solids [1–3]. One major advantage of bubble rafts is that their two-dimensional nature allows for easy imaging and tracking of all of the "particles" in the system. Another reason that bubble rafts have been so useful in the study of molecular systems is that there exist detailed calculations of the bubble interactions [30]. More recently, bubble rafts were used to study rearrangements after a step strain in order to make comparisons with the quasistatic simulations of foam [4]. This work did not directly measure T1 events, but it did look at changes in the number of neighbors for bubbles. The results suggested that large-scale events were possible.

Experiments have also been carried out using monolayer foam [31]. Langmuir monolayers consist of a single layer of

molecules confined to the air-water interface. They exhibit a large number of two-dimensional phases, including gas-liquid coexistence. This allows for the formation of a foam of gas bubbles with liquid walls. For a monolayer foam under steady shear, only a small number of simultaneous T1 events were observed, with $R_{T1}=0.12\pm0.03$. These results are consistent with the bubble model.

As mentioned, the other aspect of T1 dynamics is their potential role in explaining shear localization in yield-stress materials [23], such as foam and granular systems. It has long been known that a yield stress and/or nonlinear viscosity can lead to inhomogeneous flows [32]. However, it is only recently that experimental techniques have allowed for detailed measurements of such behavior. A number of such studies have been carried out in granular materials, where exponential velocity profiles (or other strongly localized velocity profiles) are generally observed [33–35]. In contrast, measurements in various three-dimensional pastes, slurries, and foams show a different type of inhomogeneous flow. In this case, the flow is not strongly localized, and there is a shear discontinuity at the boundary between flow and no flow [36,37].

For two-dimensional foams, the situation is ambiguous. Three-dimensional foam that is confined between plates to form a model two-dimensional system (Hele-Shaw cell geometry) exhibits shear localization analogous to granular systems [38]. This work motivated simulations of the modified vertex model discussed earlier that showed a connection between T1 events and shear localization [23]. In this case, it appears that the spatial distribution of stress released by a T1 event results in the subsequent localization of the events. The localization of T1 events is correlated with the localization of flow. In contrast, experiments with a bubble raft exhibit a shear discontinuity [39] similiar to that reported in Refs. [36,37]. In Ref. [39], T1 events were not measured. It is not surprising that there are differences between results for bubble rafts and the Hele-Shaw geometry. Because of the boundary conditions on the bubbles, the two systems possess different dissipation mechanisms. This can lead to differences in the interactions between T1 events.

The work reported in this paper addresses the general question of the temporal and spatial distribution of T1 events during the slow, steady shear of a bubble raft. Also, connections between the T1 events and the velocity profiles reported in Ref. [39] are made. The rest of the paper is organized as follows. Section II provides the details of the experimental setup. The results are presented in two parts. Section III A presents the initial response of the system. Section III B presents the behavior during plastic flow. Finally, the results are summarized and discussed in Sec. IV.

II. EXPERIMENTAL METHODS

The experimental system consisted of a standard bubble raft [1] in a Couette geometry. The bubble raft was produced by flowing regulated nitrogen gas through a hypodermic needle into a homogeneous solution of 80% by volume deionized water, 15% by volume glycerine, and 5.0% by volume Miracle Bubbles (Imperial Toy Corp.). The bubble size was dependent on the nitrogen flow rate, which was varied using a needle valve. A random distribution of bubble sizes was used, with an average radius of 1 mm. The resulting bubbles were spooned into a cylindrical Couette viscometer. This produced a two-dimensional model of a wet foam on a homogeneous liquid substrate. Figure 2 presents a schematic side view of the bubbles in the apparatus and an image of a top view of the bubble raft.

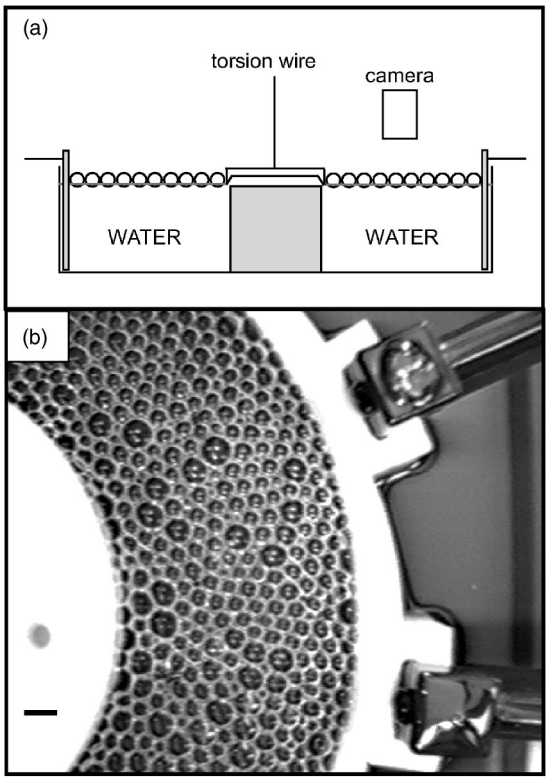

FIG. 2. (a) A schematic drawing of the apparatus showing a side view. The main elements of the apparatus are the knife edge disk that is supported by a torsion wire and that serves as the inner cylinder for the bubbles. There is a separate fixed inner cylinder in the fluid (in gray). There is a segmented outer cylinder for generating flow, and there is a fixed dish that holds the fluid. The bubbles sit on top of the fluid, as indicated by the circles. (b) An image from the top of the bubbles in the apparatus that shows a portion of both the outer and inner cylinder. The black scale bar in the lower left corner is 5 mm.

Due to the nature of the bubble raft, no measurable coarsening was observed. However, after approximately two hours, significant numbers of bubbles would pop, presumably due to loss of fluid in the walls. This set the upper limit on the total time of the measurements. In contrast, during the initial two-hour period, only two out of approximately 400 bubbles in the field of view were observed to pop.

An important feature of the bubble raft is the gas area fraction. To achieve a desired gas area fraction, the bubble raft was constructed by placing the approximate number of desired bubbles in the trough with the outer barrier set to a large radius. It is important to note that the bubbles exhibited a strong attraction to each other. The outer barrier was compressed until the desired radius was reached. The gas area fraction was determined by thresholding images of the

bubbles and counting the area inside of the bubbles. Because of the three-dimensional nature of the bubbles, this represents an operational definition of gas-area fraction based on the details of the image analysis. However, the choice of threshold was consistent with an estimate of the gas area fraction based on the area of trough and expected distribution of bubble sizes. For all of the data reported here, the gas area fraction was approximately 0.95.

The Couette viscometer is described in detail in Ref. [40] and shown schematically in Fig. 2(a). It consists of a shallow dish that contains the liquid substrate. Two concentric Teflon barriers are placed vertically in the dish. Sections of both of these barriers are visible in Fig. 2(b). The outer barrier is a ring consisting of 12 segmented pieces. It has an adjustable radius. For the experiments discussed here, the outer radius was fixed at $r_o = 7.43$ cm. The inner barrier, or rotor, is a Teflon disk with a radius $r_i = 3.84$ cm. The outer edge of the disk is a knife edge that is just in contact with the water surface. It was suspended by a wire to form a torsion pendulum.

To shear the bubble raft, the outer Teflon barrier was rotated at a constant angular velocity $\Omega = 8 \times 10^{-4}$ rad/s. The first layer of bubbles at either boundary did not slip relative to the boundary. Due to the finite size of the bubbles, this results in an effective inner radius of $r = 4.4$ cm. Due to the cylindrical geometry, the shear rate is not uniform across the system and is given by $\dot{\gamma}(r) = r(d/dr)[v(r)/r]$. Here $v(r)$ is the azimuthal velocity of the bubbles. During plastic flow, the average azimuthal velocity of the inner cylinder is zero. Measurements of the average azimuthal velocity profile allow for calculations of the shear rate. As measured at $r = 4.4$ cm, $\dot{\gamma} = 4 \times 10^{-3}$ s^{-1}. In this regime, where reported, the strain (γ) is taken to be the strain at this radius, and is computed from $\gamma = \dot{\gamma} t + \gamma_o$, where t is the time since the initiation of plastic flow and γ_o is the amount of strain developed during the initial period. During the initial period, the inner barrier has a finite angular speed. However, one can still compute the effective shear rate at $r = 4.4$ cm. In this regime, $\dot{\gamma} = 3 \times 10^{-4}$ s^{-1}. Again, where reported, the strain is the strain at the inner cylinder: $\gamma = \dot{\gamma} t$, where in this case t is measured from the initiation of shear.

The details of the velocity measurements are given in Ref. [39]. Video tape of roughly one-third of the trough was recorded. Images from this tape were taken every 3.2 s and digitized. An image-processing routine based on standard LABWINDOWS functions was developed that detected and tracked individual bubbles. This tracking software was also used to compute the average bubble displacements. This is used to compute the deviation of the bubble motion from ideal elastic behavior, as discussed in Sec. III A.

The T1 events were measured by stepping the digitized images one frame at a time and visually searching for the location and time at which T1 events occurred. A T1 event was defined to occur when two bubbles were observed to lose contact, and two other bubbles moved into the resulting space (see Fig. 1). Due to the associated motions of the other neighboring bubbles, T1 events are relatively easy to detect by hand [41]. For automatic tracking of T1 events, it is critical to accurately detect essentially all of the bubbles, as one is interested in determining neighbor switching events. This is in contrast with the displacement and velocity measurements where the requirement is that one tracks enough bubbles to have sufficient statistics. These are the reasons that automatic methods were used for displacement and velocity measurements and that T1 events were detected by hand.

The stress on the inner rotor was determined using two different methods. In both cases, the torque, $T = \kappa\theta$, on the inner rotor is determined by measuring the angular displacement, θ. (For the experiments presented here, the torsion constant $\kappa = 5.7 \times 10^{-7}$ N m.) The stress is then determined from $\sigma = T/2\pi r^2$. The difference in the two methods is the determination of θ. The first method uses a magnetic flux technique, and the details of this technique are in Ref. [40]. This is the more precise of the two methods, with a stress resolution of 3×10^{-3} mN/m. The second method uses the video images of the inner cylinder and tracks fixed features on the disk. This method has a resolution of 0.043 mN/m. The second method is used to correlate the video analysis of bubble motions (displacements and T1 events) with the detailed stress fluctuations determined from the magnetic flux measurements that are reported in Ref. [42].

As mentioned, foams are inherently nonequilibrium systems. One complication that arises from this is the definition of the yield stress. For sufficiently low shear rates, foam will spontaneously release stress, usually as part of the coarsening process as bubble sizes change. This complication is minimized in the bubble raft given that no substantial coarsening was observed in the absence of applied shear. In either case, a useful operational definition of the yield stress is the zero shear-rate limit of the stress. For the bubble raft of interest here, the average stress as a function of shear rate is well described by a Herschel-Bulkley model $[\sigma(\dot{\gamma}) = \tau_o + \mu\dot{\gamma}^n]$ [43]. From these results, one can determine a yield stress: $\tau_o = 0.8 \pm 0.1$ mN/m [39,42]. For the particular shear rate of interest here, this is different from the "critical" stress at which the system begins to undergo "steady" flow.

III. EXPERIMENTAL RESULTS

A. Elastic regime

The initial stress response of the system is given in Fig. 3. There are a number of interesting features of this regime. First, there are three separate regions of the initial response, which is essentially set by the slope of the stress versus strain curve. These regions are separated by isolated stress drops that are indicated by the vertical dashed lines in the figure.

The first region is the linear, elastic response of the material. During this period, no T1 events are observed. The second two regions represent plastic deformations in the sense that T1 events occur. These events are too small to produce stress drops. But, they modify the slope of the stress-strain curve and generate irreversible deformation. This is the justification for identifying these regions with plastic deformations. The onset of plastic response is another useful definition of the yield stress. However, there is always ambiguity associated with the definition of the onset of T1 events due to the possibility of T1 events that are the result of coarsening and not shear. As discussed for the bubble raft, this difficulty

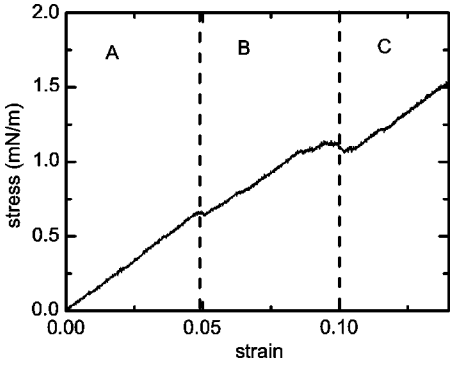

FIG. 3. Stress on the inner cylinder versus strain for the initial period of shear. The curve is divided into three regions labeled *A*, *B*, and *C*. Region *A* is the only period for which no T1 events are observed.

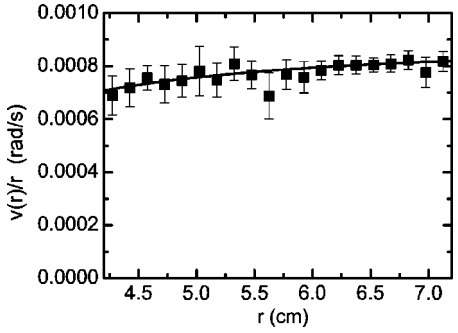

FIG. 4. A plot of $v(r)/r$ vs radial position for the bubble motion during interval *A* in Fig. 3. The solid squares are data averaged over all bubbles at a given radial position. The solid line is a fit to Eq. (4).

is minimized because no coarsening was observed. However, for the measurements in Fig. 3, only a fraction of the trough was in view. This limits the degree to which the yield stress can be measured by this method. However, it is useful to note that the onset of T1 events for the single set of data studied here is consistent with the value of yield stress as determined by fits to the behavior of stress as a function of rate of strain.

The fact that any deviation of the stress-strain curve from linear behavior is small allows for the definition of an effective shear modulus of the bubble raft, G, during periods of stress increase. For the initial region in Fig. 3, G is the elastic shear modulus. The calculation of G assumes that the stress is proportional to the strain. The boundary conditions consist of a fixed rotation rate at the outer boundary and an inner boundary that is free to rotate, but supported by a torsion wire. Because of the symmetry of the Couette geometry, the azimuthal velocity, $v(r)$, is only a function of the radial position r. This is a standard problem; however, given the slightly unorthodox boundary conditions of this experiment, the solution is repeated here. The relevant constitutive equation is

$$\sigma(r) = G\gamma(r). \tag{1}$$

Here $\gamma(r)$ is the shear strain and $\sigma(r)$ is the resulting shear stress. In the cylindrical geometry, $\gamma(r)=r[d\theta(r)/dr]$, where $\theta(r)$ is the angular displacement of the bubble raft. For a material confined between two cylinders, the shear stress is given by $\sigma(r)=T/(2\pi r^2)$. This follows directly from balancing torques on each material element. If the bubble raft was a perfectly rigid solid, one would simply have $v(r)=\Omega r$. This is due to the fact that the inner boundary is supported by a torsion wire and rotates as it measures the torque on the inner cylinder. However, for a finite value of G, plugging into Eq. (1), one gets

$$\frac{T}{2\pi r^2} = G\left(r\frac{d\theta(r)}{dr}\right). \tag{2}$$

Integrating this equation, and using the fact that the bubble raft does not slip at either boundary, gives for G,

$$G = \frac{\omega}{\Omega-\omega}\left(\frac{\kappa}{4\pi}\right)\left(\frac{1}{r_i^2}-\frac{1}{R^2}\right), \tag{3}$$

and for v,

$$v(r) = \Omega r - \left[\frac{\kappa\omega r}{4\pi G}\left(\frac{1}{r^2}-\frac{1}{R^2}\right)\right]. \tag{4}$$

This equation for v can be rewritten by plugging in for G,

$$v(r) = \Omega r + \left[\frac{(\Omega-\omega)r_i^2}{R^2-r_i^2}\left(r-\frac{R^2}{r}\right)\right]. \tag{5}$$

The second piece in the expressions for $v(r)$ is due to the elastic nature of the bubble raft and the motion of the inner cylinder. When κ/G is small, the system behaves as a rigid body ($\omega=\Omega$), as expected (large-G limit).

Using the above results, one can find G from measurements of the average velocity using Eq. (4) or from ω using Eq. (3). For example, the results for $v(r)$ in region *A* of Fig. 3 are given in Fig. 4. The solid line is a fit to Eq. (4), with $v(r)/r=8.2\times10^{-4}$ rad/s -0.003 rad/cm^2 s $(1/r^2 - 0.0193$ cm$^{-2})$. The T1 events result in a reduction in the effective elastic modulus of the bubble raft. The calculated values of G for the three regions are: (*A*) $G=11.2\pm0.1$ mN/m; (*B*) $G=5.4\pm0.1$ mN/m; and (*C*) $G=8.9\pm0.1$ mN/m.

I used the elastic regime to provide a characterization of the local deviation from elastic flow. First, the fit of $v(r)$ in region *A* is used as the definition of "ideal" elastic motion. Knowing this velocity curve, the expected displacement of a bubble during a strain interval can be computed. From this, Δ is defined to be a measure of the deviation from elastic behavior: $\Delta=\sqrt{(x-x_e)^2+(y-y_e)^2}$, where x and y are the actual displacements of the bubble and x_e and y_e are the expected displacements if the motion was "ideal" elastic behavior. As can be seen from Fig. 4, even in the "pure elastic" regime there is a significant nonzero variation to the bubble motions. (The error bars represent the standard error based on the standard deviation of measured velocities in each radial bin.) The variation in bubble velocity is due to a combination of effects, including the obvious fact that one expects a distribution of displacements due to the finite size of

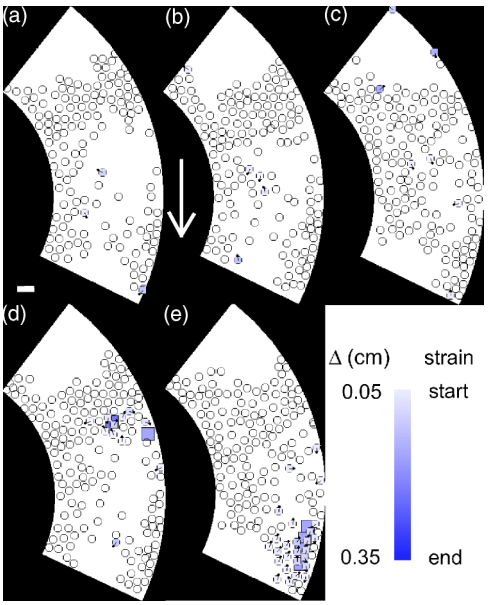

FIG. 5. (Color online) Five images representing typical bubble deviations from elastic flow during the initial stress rise. The arrow in image (a) gives the direction of rotation of the outer cylinder. Images (a)–(c) are taken from the corresponding three strain intervals in Fig. 3 and show typical strain intervals in which no T1 events occur. Image (d) shows a typical localized T1 event from region *B* in Fig. 3. Image (e) shows an event composed of multiple T1 events in which two rows of bubbles slip pass each other. This event is taken from region *C* in Fig. 3. The circles indicate the location of a subset of bubbles that have been tracked. The sizes of all the circles are the same, independent of actual bubble size, for clarity. They are grayscaled (color-coded) based on the deviation from elastic displacements, as defined in the text. White represents deviations less than 0.05 cm. The grayscale (color) bar gives the scale for deviations greater than 0.05 cm. The solid line associated with bubbles gives the direction of the deviation from elastic displacements. The squares represent the location of T1 events, where the grayscale (color) represents the time relative to the start of the strain interval used to calculate Δ. The scale bar in image (a) is 0.5 mm.

the bubbles. Therefore, the variation in displacements from the ideal elastic behavior in region *A* is used to set a minimum threshold value for Δ of 0.05 cm. Bubbles with a value of Δ below this threshold are considered to have undergone "elastic" motion. Even with this cutoff, there are a small number of bubbles in the tails of the distribution that are classified as deviating from elastic behavior even in region *A*. Values of Δ and the spatiotemporal location of T1 events are illustrated in Fig. 5 for a selected set of bubbles. Figures 5(a)–5(c) illustrate the value of Δ computed over a period of strain of 0.064 in which no T1 events occur. Each period of strain is a small subset of the corresponding strain interval (*A*, *B*, or *C*) of Fig. 3. The circles indicate the location of tracked bubbles (so only a fraction of the total bubbles are shown). The grayscale (color) of the bubbles indicates the deviation from elastic behavior, with white bubbles having a value of $\Delta < 0.05$ cm. The grayscale (color) code is indicated in the figure. In addition, the direction of the deviation from elastic behavior is indicated by a line with a dot at the end.

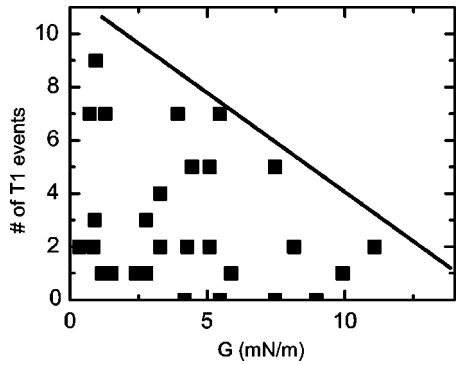

FIG. 6. Scatter plot of the number of T1 events during a period of stress increase vs the effective elastic modulus *G* for the same period of strain. The solid line is a guide to the eye.

Figures 5(d) and 5(e) illustrate two classes of T1 events that do not result in a stress drop. The spatial location of T1 events is given by squares. The timing of the T1 events, relative to the period of strain used to compute Δ, is given by the the grayscale (color) of the squares. Figure 5(d) is from region *B* of Fig. 3. This illustrates an isolated pair of T1 events that have an associated region in which the bubbles deviate from elastic behavior. Figure 5(e) is from region *C* of Fig. 3. This illustrates the slippage of two, short rows of bubbles due to simultaneous T1 events. This is made especially clear by the directions of the deviations. The planes of bubbles on either side of the T1 events move in opposite directions. Again, there is a relatively localized region of deviation from elastic behavior associated with these T1 events.

B. Plastic flow regime

In the plastic flow regime, there are two main questions regarding the T1 events. First, what is the correlation between T1 events and stress? Second, what is the correlation between T1 events and bubble motion, as measured by either the average velocity or the deviation from elastic behavior?

Regarding the correlation between T1 events and stress, it is interesting to consider the periods of stress increase. As with regions *B* and *C* in Fig. 3, there are often T1 events during these periods of stress increase. Therefore, in general, these are periods of plastic deformation, though preliminary observations suggest that occasional increases exist during which no T1 events occur. One way to characterize stress increases is to use Eq. (3) to calculate an effective shear modulus, *G*, for each separate period of stress increase. This can then be correlated with the number of T1 events that occur in that period. A preliminary measurement of this is shown in Fig. 6. This result is preliminary because only a fraction of the sample was viewed. Therefore, the results for the number of T1 events represent a lower bound. However, it is interesting that the data all fall below the straight line, suggesting a correlation between *G* and the number of T1 events, as expected.

It is natural to expect that one necessary condition for a T1 event to occur is that the local stress exceeds some critical value. This would suggest a correlation between the

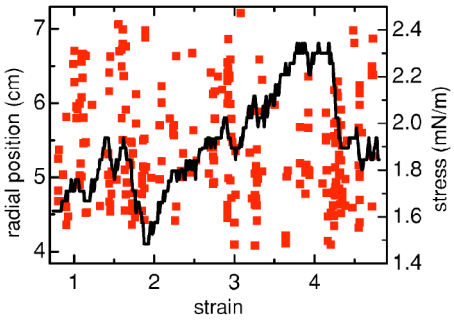

FIG. 7. The individual points are the radial position of T1 events as a function of strain. The solid curve is the stress as a function of strain (measured using images of the inner cylinder).

stress and the location of the T1 events. Figure 7 illustrates that no correlation exists between the stress on the *inner cylinder* and the radial positions of T1 events. One would expect such a correlation if the stress field was given by the continuum limit, which in a Couette geometry is $\sigma(r) = [\sigma(r_i) r_i^2]/r^2$, and the critical stress for a T1 event was spatially uniform. Under these conditions, for each $\sigma(r_i)$, there is a maximum r at which T1 events can occur. This is set by the critical stress required for the generation of a T1 event. The lack of a correlation suggests that at least one, if not both, of these assumptions is false. In fact, work in other systems suggests that both assumptions are false. Given the direct measurement of stress chains in granular matter [35], it is reasonable to expect such chains in the bubble raft. This would represent a breakdown of the continuum assumption for the stress distribution. Also, simulations of amorphous metals have shown the existence of localized, high stress regions (referred to as τ defects) that are the sources of local flow [13]. In other contexts, models and simulations have suggested the existence of "weak" zones in complex fluids [44–46] that are the source of viscouslike behavior. A more detailed study of these issues will require improved images, but the current work is very suggestive.

To summarize the average properties of T1 events as a function of strain, Fig. 8 plots the number of T1 events per bubble versus strain. Again, this is shown simultaneously with the stress versus strain curve to illustrate the general correlation between the size of the stress drops and the total number of T1 events. One observes that most stress drops

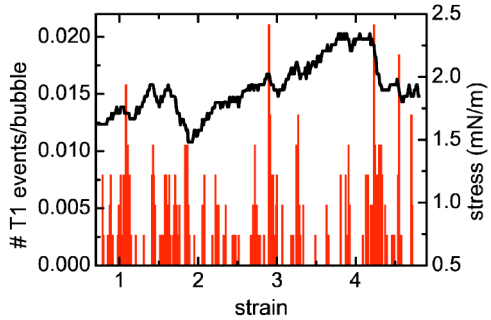

FIG. 8. The solid line is the same stress vs strain curve as shown in Fig. 7. The bars summarize the data in Fig. 7 by plotting only the number of T1 events/bubble in a strain interval of 0.013.

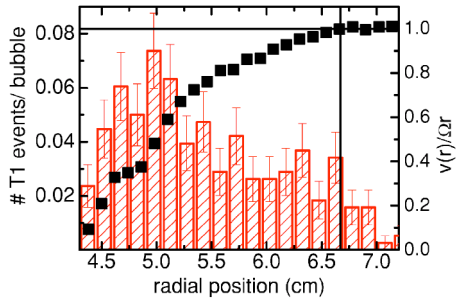

FIG. 9. The squares are the average velocity of the bubbles normalized by Ωr as a function of radial position. The bars give the total number of T1 events/bubble as a function of radial position. The solid lines are guides to the eye. The horizontal line is $v(r)/\Omega r = 1$, which corresponds to the motion of a rigid body. The vertical line is the location of the shear discontinuity, as reported in Ref. [39].

consist of a cascade of events throughout the stress drop. As with the stress increases, detailed correlations between the size of a stress drop and the number of T1 events will require images of the entire sample. However, one can compute R_{T1}. For this shear rate, $R_{T1} = 0.18 \pm 0.01$, in reasonable agreement with both the bubble model and Langmuir monolayer foam.

The next question is the connection between velocity profiles and T1 events. Based on the results of Ref. [39], it is known that there exists a shear discontinuity at $r_c = 6.7$ cm for the system reported on here. Therefore, there is no expectation of strong localization of the T1 events as reported in Ref. [23] because there is no shear localization. However, one might expect a connection between the radial distribution of T1 events and the shear discontinuity.

The shear discontinuity divides the system into two regimes. Below r_c, the average velocity is consistent with that of a power-law fluid. Above r_c, the system acts like an elastic solid. Figure 9 illustrates the connection between the average velocity profile and the spatial distribution of T1 events. The vertical line indicates the spatial location of the shear discontinuity [39]. The basic shape of the distribution is similar to that found in the simulations reported in Ref. [23]. There is a "peak" at smaller radii, with the distribution tailing off as one goes to larger radii. The main difference is the location of the cutoff in the T1 distribution. As reported in Ref. [23], the cutoff in velocity and T1 events is at essentially the same radius. In contrast, for the system reported on here, there is no obvious signature in the distribution of T1 events at the shear discontinuity (see Fig. 9). This may be due to the fact that even though the shear-rate is zero, the bubbles are still moving near the outer wall, and differences in bubble size may lead to T1 events. Also, it may be an artifact of how close the shear discontinuity is to the outer wall. Future work in larger systems is needed to better understand this issue.

In order to better understand the detailed connection between T1 events and stress drops, two short periods of strain are highlighted, as indicated in Fig. 10. These are segments of the data presented in Fig. 7. The period of strain illustrated in Fig. 10(a) was selected to highlight the nature of potential correlations between the stress behavior and the number of T1 events. First, the initial elastic rise A is included for com-

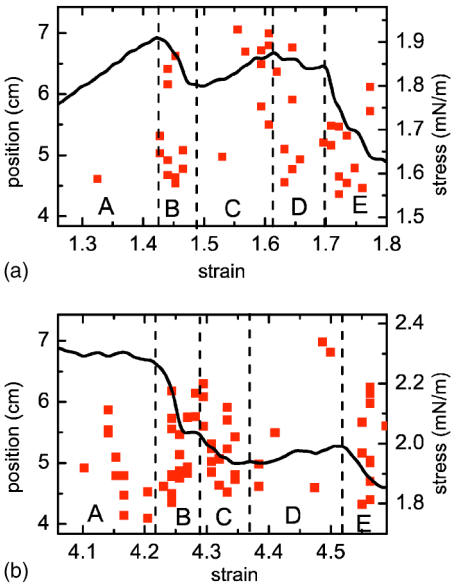

FIG. 10. This is two strain intervals from Fig. 7, showing both the location of T1 events (solid squares) and the stress (solid line, as measured by the magnetic method) as a function of strain. Each interval is further divided into smaller strain intervals by the vertical lines. The labels in (b) correspond to the images in Fig. 11.

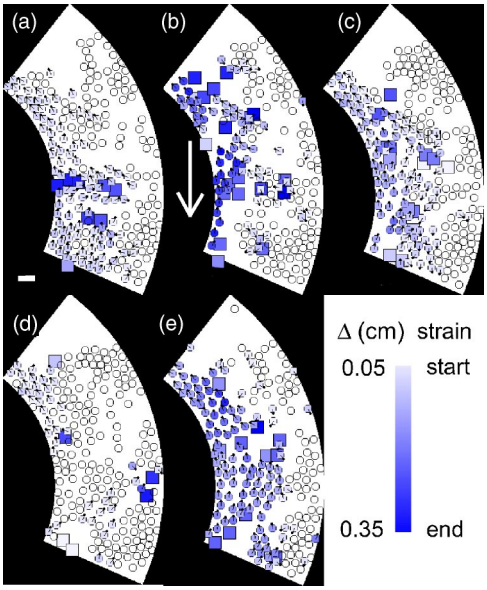

FIG. 11. (Color online) Five images representing typical bubble deviations from elastic flow during the corresponding strain intervals as indicated in Fig. 10(b). The arrow in image (a) gives the direction of rotation of the outer cylinder. The circles indicate the location of a subset of bubbles that have been tracked. The size of the circle is the same for all bubbles for clarity. The circles are grayscaled (colored) based on the deviation from elastic displacements, as defined in the text. White represents deviations less than 0.05 cm. The bar gives the scale for deviations greater than 0.05 cm. The solid line associated with bubbles gives the direction of the deviation from elastic displacements. The squares represent the location of T1 events, where the grayscale (color) equals the time relative to the start of the strain interval used to calculate Δ. The scale bar in image (a) is 0.5 mm.

parison with the stress increase in the interval labeled *C*. During the initial rise, there is only one observed T1 event, and the effective elastic modulus is $G=5.6\pm0.1$ mN/m. In contrast, during region *C*, there are nine observed T1 events, and the effective elastic modulus is $G=2.1\pm0.1$ mN/m. These results reinforce the general connection between number of T1 events and effective elastic modulus discussed with respect to Fig. 6. In contrast, the regions labeled *B*–*E* all have roughly the same number of T1 events, yet regions *B* and *E* are stress drops. Region *C* is a period of stress increase, and region *D* is a slight decrease in stress. One difficulty in drawing definitive conclusions from these data is the fact that only part of the system is being viewed. However, this strongly suggests that the additional bubble motions, not just the T1 events, play an important role in determining the overall stress evolution.

The interval illustrated by Fig. 10(b) was selected to make connections with the velocity profiles reported in Ref. [39] in an attempt to better understand the shear discontinuity that occurs at r_c. Here, the average bubble displacements are measured during a fixed interval in time. These are directly related to average velocities. This sequence is particularly interesting because there are three stress drops that occur at different average stress values, and the drop at the lowest average stress (region *E*) exhibits the largest value of r_c [39]. (I am considering the behavior in regions *B* and *C* as two separate stress drops because of the short plateau between them. However, this points out the issue regarding the definition of "events" as discussed earlier in the context of Ref. [29].)

The spatiotemporal distribution of T1 events and values of bubble deviations from elastic behavior for a particular strain interval (Δ) are given in Fig. 11 using the same criteria as described for Fig. 5 in Sec. III B. White bubbles represent essentially elastic behavior, and the grayscale (color) of the other bubbles is the degree to which their motion deviates from elastic. The solid line associated with shaded bubbles gives the direction of the deviation from elastic displacements. The timing of the T1 events, relative to the period of strain used to compute Δ, is given by the grayscale (color) of the squares.

It should be noted that the spatial organization of the directions of the displacements is suggestive of large-scale structure in the deviations similar to that reported elsewhere [38,47,48]. For each image in Fig. 11, Δ is calculated for the corresponding strain interval in 10(b). For example, Fig. 11(a) represents the values of Δ and the spatiotemporal location of T1 events for region *A* of Fig. 10(b). One observes very similar distributions of T1 events for all three stress drops [see Figs. 11(b), 11(c), and 11(e)]. If one looks carefully, the distinguishing factor appears to be the number of bubbles deviating from elastic behavior at any given radius. This is made clearer by considering the average bubble displacement as a function of radial position, as illustrated in Fig. 12.

Figure 12 is a plot of $\Delta\theta/\Omega\Delta t$ versus radial position. The values of $\Delta\theta$ are computed by dividing the system into 20 equally spaced radial bins and averaging the angular displacements over all bubbles in a given bin over the time

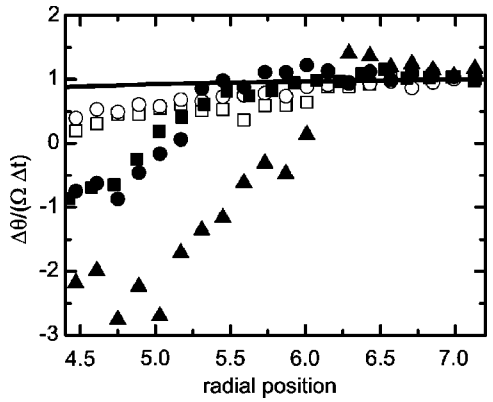

FIG. 12. The average angular displacement of the bubbles normalized by $\Omega\Delta t$ as a function of radial position. The different symbols are for the different strain intervals in Fig. 10(b): (a) open circles; (b) solid squares; (c) solid circles; (d) open squares; and (e) solid triangles. Here Δt is the time interval for each strain interval. The solid line is the fit to elastic behavior from Fig. 4.

interval of interest. The time intervals are selected so that they match the strain intervals indicated in Fig. 10(b). For comparison, the displacements during the essentially flat regions in stress are given as open symbols, and the displacements during the stress drops are given as closed symbols. The angular displacement is normalized by $\Omega\Delta t$. The solid line is the "ideal" elastic behavior given by the fit to the data in Fig. 4. One can see that for interval *E* (solid triangles), the deviation from the expected elastic displacement occurs at the largest value of *r*. This is consistent with the results reported in Ref. [39] for the velocity profiles. What is new in these results is the ability to correlate the location of T1 events during a stress drop and the location of the deviation from elastic behavior.

For event *E*, there are two clear deviations from elastic behavior, as shown in Fig. 12: (a) at $r=6.48$ cm there is a positive deviation, and (b) at $r=6.16$ cm there is a negative deviation. During the drop, the maximal radial position of a T1 event is $r=6.24$ cm. The existence of positive and negative deviations is consistent with the bubbles associated with a T1 event moving both forward and backward relative to the average flow. The average displacements during *B* and *C* are essentially identical. However, for *C* more than *B* there is some evidence for a positive and negative deviation at $r=5.84$ cm and at $r=5.44$ cm, respectively. For these drops, the maximal radial position of a T1 event is $r=6.29$ cm. Comparing these numbers strongly suggests that the location of T1 events is not the main contribution to the determination of the deviation from elastic behavior, and hence, the determination of r_c. Instead, it is the detailed motion of the surrounding bubbles. Interestingly, the greatest difference between the two events in terms of T1 position is in the precursor to the drops; yet the precursors have very similar angular displacements (open symbols in Fig. 12). During the interval labeled *D* in Fig. 10(b), one observes T1 events as far out as $r=6.98$ cm. In contrast, during the interval labeled *A* in Fig. 10(b), one only observes T1 events as far out as $r=5.87$ cm. Presumably, these events play an important role in establishing the local stress fields that govern the bubble motions during the subsequent stress drop.

IV. DISCUSSION

Even though various aspects of the work presented here are preliminary in the sense that only a portion of the entire raft was studied, a number of questions regarding the role of T1 events in the macroscopic response of a bubble raft to flow have been addressed. First, the contribution of T1 events to the effective shear modulus was considered. T1 events during periods of increasing stress effectively lower the shear modulus of the bubble raft. Similarly, during stress drops, there is a correlation between the size of the drop and the total number of T1 events. Future work is required to establish a more detailed correlation between the number of T1 events and the effective shear modulus and size of stress drops.

Correlations between positions of T1 events, average stress, individual bubble displacements, and average angular displacements of bubbles were considered. A general picture that emerges from these measurements is the importance of understanding the local stress field and the local geometry of bubbles. For example, an investigation of individual bubble motions before and during a stress drop (see discussion of Figs. 10 and 11) shows that the radial distribution of T1 events cannot be understood in terms of a simple continuum model and single stress threshold. The T1 events in the strain period immediately prior to a stress drop play an important role in establishing the local stress field and geometric relations between bubbles that set the subsequent motions. For example, the two different stress drops highlighted in Fig. 10 exhibited similar distributions of T1 events, but the deviations from elastic behavior and the average displacements were very different. The main differences between the events was in the distribution of precursor T1 events, not in the average bubble motions.

The connection between T1 events and the position of the shear discontinuity was also considered, both in terms of the average properties (see Fig. 9) and the short time motions (see Fig. 12). There is no clear evidence for a connection between the positions of T1 events and the shear discontinuity, but larger system sizes need to be studied. However, there may be an indirect connection through the stress relaxation and subsequent motion of surrounding bubbles. Indirectly, these measurements have some potential implications for the simulations of the modified vertex model [23]. These simulations illustrate that a localization of T1 events can lead to a shear localization. This system does not exhibit localization of either the T1 events or the shear. This indirectly supports the connection between T1 event localization and shear localization. What remains an important question is why would T1 events localize in one case and not the other? An obvious difference between the T1 events in the bubble raft and in the simulation is the duration of the T1 events. In the model, the T1 events all occur on a very short time scale, by construction. For the bubble raft, there is a distribution of times for the duration of T1 events. Some events occur very slowly (over 10–20 s). As mentioned in the Introduction, these differences in time scales are not surprising given the different dissipation mechanisms in the bubble raft and the Hele-Shaw cell. However, it is interesting to explore how these differences in duration of T1 events modify local stress

variations. Again, this points to the importance of understanding the local stress fields generated by the T1 events, and not just the distribution of the events themselves. Furthermore, as part of the future work that focuses on local stress fields, it will be important to correlate the changes in local stress with the duration of the T1 events.

The measurements reported here focused on bubble displacements and T1 events. Where possible, comparisons with the bubble model show quantitative agreement, such as for R_{T1}. This adds support to previous results with the bubble raft that were also in general agreement with the bubble model [5,42]. Having strong agreement between the experiments and a theoretical model is useful for the next stage of experimental studies. Essentially all of the results point to the need for measurements of the local stress field. Future experimental work is planned that will use the bubble distortion as a direct measure of local stress, as has been done with other foam systems [49–52]. Close contact with simulations that focus on the stress released by T1 events and STZ's, as well as experimental studies of granular material, will be important for understanding this future work.

ACKNOWLEDGMENTS

This work was supported by the Department of Energy Grant No. DE-FG02-03ED46071, the Research Corporation, and the Alfred P. Sloan Foundation. I thank John Lauridsen for use of his video data of bubble rafts. I thank Craig Maloney, Corey O'Hern, Michael Falk, and Georges Debrégeas for fruitful discussions.

[1] A. S. Argon and H. Y. Kuo, Mater. Sci. Eng. **39**, 101 (1979).
[2] L. Bragg and W. M. Lomer, Proc. R. Soc. London, Ser. A **196**, 171 (1949).
[3] D. Mazuyer, J. M. Georges, and B. Cambou, J. Phys. (France) **49**, 1057 (1989).
[4] A. AbdelKader and J. C. Earnshaw, Phys. Rev. Lett. **82**, 2610 (1999).
[5] J. Lauridsen, M. Twardos, and M. Dennin, Phys. Rev. Lett. **89**, 098303 (2002).
[6] M. L. Falk and J. S. Langer, Phys. Rev. E **57**, 7192 (1998).
[7] A. Onuki, Phys. Rev. E **68**, 061502 (2003).
[8] G. Picard, A. Ajdari, F. Lequeux, and L. Bocquet, e-print cond-mat/0403647.
[9] V. V. Bulatov and A. S. Argon, Modell. Simul. Mater. Sci. Eng. **2**, 167 (1994).
[10] V. V. Bulatov and A. S. Argon, Modell. Simul. Mater. Sci. Eng. **2**, 185 (1994).
[11] V. V. Bulatov and A. S. Argon, Modell. Simul. Mater. Sci. Eng. **2**, 203 (1994).
[12] J. C. Baret, D. Vandembroucq, and S. Roux, Phys. Rev. Lett. **89**, 195506 (2002).
[13] D. Srolovitz, V. Vitek, and T. Egami, Acta Metall. **31**, 335 (1983).
[14] K. Kawasaki, T. Nagai, and K. Nakashima, Philos. Mag. B **60**, 399 (1989).
[15] K. Kawasaki, T. Okuzono, T. Kawakatsu, and T. Nagai, in *Proceedings of the International Workshop of Physics of Pattern Formation*, edited by S. Kai (World Scientific, Singapore, 1992).
[16] T. Okuzono and K. Kawasaki, Phys. Rev. E **51**, 1246 (1995).
[17] D. J. Durian, Phys. Rev. Lett. **75**, 4780 (1995).
[18] D. J. Durian, Phys. Rev. E **55**, 1739 (1997).
[19] D. Weaire, F. Bolton, T. Herdtle, and H. Aref, Philos. Mag. Lett. **66**, 293 (1992).
[20] S. Hutzler, D. Weaire, and F. Bolton, Philos. Mag. B **71**, 277 (1995).
[21] Y. Jiang, P. J. Swart, A. Saxena, M. Asipauskas, and J. A. Glazier, Phys. Rev. E **59**, 5819 (1999).
[22] S. Tewari, D. Schiemann, D. J. Durian, C. M. Knobler, S. A. Langer, and A. J. Liu, Phys. Rev. E **60**, 4385 (1999).
[23] A. Kabla and G. Debrégeas, Phys. Rev. Lett. **90**, 258303 (2003).
[24] J. Stavans, Rep. Prog. Phys. **56**, 733 (1993).
[25] A. M. Kraynik, Annu. Rev. Fluid Mech. **20**, 325 (1988).
[26] D. Weaire and S. Hutzler, *The Physics of Foams* (Clarendon Press, Oxford, 1999).
[27] A. S. Argon, Acta Metall. **27**, 47 (1979).
[28] D. L. Malandro and D. J. Lacks, J. Chem. Phys. **110**, 4593 (1999).
[29] C. Maloney and A. Lemaître, e-print cond-mat/042148.
[30] L. T. Shi and A. S. Argon, Philos. Mag. A **46**, 255 (1982).
[31] M. Dennin and C. M. Knobler, Phys. Rev. Lett. **78**, 2485 (1997).
[32] Various books cover both the modeling and experimental measurement of yield stress materials, and complex fluids in general. Two examples are R. B. Bird, R. C. Armstrong, and O. Hassage, *Dynamics of Polymer Liquids* (Wiley, New York, 1977) and C. Macosko, *Rheology Principles, Measurements, and Applications* (VCH Publishers, New York, 1994).
[33] W. Losert, L. Bocquet, T. C. Lubensky, and J. P. Gollub, Phys. Rev. Lett. **85**, 1428 (2000).
[34] D. M. Mueth, G. F. Debregeas, G. S. Karczmar, P. J. Eng, S. R. Nagel, and H. M. Jaeger, Nature (London) **406**, 385 (2000).
[35] D. Howell, R. P. Behringer, and C. Veje, Phys. Rev. Lett. **82**, 5241 (1999).
[36] P. Coussot, J. S. Raynaud, F. Bertrand, P. Moucheront, J. P. Guilbaud, H. T. Huynh, S. Jarny, and D. Lesueur, Phys. Rev. Lett. **88**, 218301 (2002).
[37] F. DaCruz, F. Chevoir, D. Bonn, and P. Coussot, Phys. Rev. E **66**, 051305 (2002).
[38] G. Debrégeas, H. Tabuteau, and J. M. di Meglio, Phys. Rev. Lett. **87**, 178305 (2001).
[39] J. Lauridsen, G. Chanan, and M. Dennin, Phys. Rev. Lett. **93**, 018303 (2004).
[40] R. S. Ghaskadvi and M. Dennin, Rev. Sci. Instrum. **69**, 3568 (1998).
[41] The detection of T1 events by hand was tested using data generated based on the bubble model. The number of T1 events detected by hand and with the computer agreed well within expected statistical errors.

[42] E. Pratt and M. Dennin, Phys. Rev. E **67**, 051402 (2003).
[43] R. B. Bird, R. C. Armstrong, and O. Hassuage, *Dynamics of Polymer Liquids* (Wiley, New York, 1977).
[44] A. J. Liu, S. Ramaswamy, T. G. Mason, H. Gang, and D. A. Weitz, Phys. Rev. Lett. **76**, 3017 (1996).
[45] P. Sollich, F. Lequeux, P. Hébraud, and M. E. Cates, Phys. Rev. Lett. **78**, 2020 (1997).
[46] S. A. Langer and A. J. Liu, J. Phys. Chem. B **101**, 8667 (1997).
[47] A. Tanguy, J. P. Wittmer, F. Leonforte, and J.-L. Barrat, Phys. Rev. B **66**, 174205 (2002).
[48] F. Radjai and S. Roux, Phys. Rev. Lett. **89**, 064302 (2002).
[49] D. A. Reinelt and A. Kraynik, J. Rheol. **44**, 453 (2000).
[50] M. Aubout, Y. Jiang, J. A. Glazier, and F. Graner, Granular Matter **5**, 67 (2003).
[51] E. Janiaud and F. Graner, e-print cond-mat/0306590.
[52] R. C. Ball and R. Blumenfeld, Phys. Rev. Lett. **88**, 115505 (2002).